Vol. 03, Iss. 3 (2025) 259-284, DOI: 10.61552/JME.2025.03.002

Journal of Materials and Engineering

www.jme.aspur.rs

Research article

Optimum Selection of Magnetic Abrasive Flow Machining Conditions During Finishing of Al/SiC/B_4C–MMCs Using Taguchi's Technique

Gagandeep Chawla[a, *]

[a]*Department of Mechanical Engineering, Seth Jai Parkash Mukand Lal Institute of Engineering and Technology (JMIT), Radaur-135133, YamunaNagar, (Haryana), India.*

Keywords:

MAFM
Al / SiC / B_4C - MMCs
MRR
ΔRa
SEM
ANOVA
Taguchi method

* Corresponding author:

Gagandeep Chawla
E-mail: gagan1984mech@gmail.com

Received: 14 July2024
Revised: 21 August 2024
Accepted: 23 September 2024

A B S T R A C T

The use of non-conventional finishing processes for composite materials is essential as these materials have supplanted the conventional ones in several applications as they have properties such as lightweight, high strength and good economy. The current investigation attempts to finish the hybrid Al/SiC/B_4C MMCs using magnetic abrasive flow machining (MAFM) process. The Taguchi L_{27} orthogonal array is designed for experimentation to study the impact of input factors on change in surface roughness (ΔR_a), material removal rate (MRR) and surface morphology. Magnetic flux density (M_f), workpiece material (W_p), mesh number (M), concentration of abrasives (C), extrusion pressure (E_p) and number of cycles (N) are considered as the process variables. Analysis of means of data and ANOVA is employed to find the impact of the process factors on MRR and ΔR_a. The optimal level of process factors for achieving better MRR has been obtained as magnetic flux density (M_f) = 0.45 Tesla, workpiece material (W_p) = 3, mesh number (M) = 150, concentration of abrasives (C) = 50, extrusion pressure (E_p) = 7 Mpa and number of cycles (N) = 200. Moreover, the optimal level of process parameters for achieving better ΔR_a has been obtained as magnetic flux density (M_f) = 0.45 Tesla, workpiece material (W_p) = 2, mesh number (M) = 220, concentration of abrasives (C) = 50, extrusion pressure (E_p) = 7 Mpa and number of cycles (N) = 100. It has been observed that extrusion pressure and magnetic flux density are the most significant variables in regard to MRR and ΔR_a. The surface morphology of finished and unfinished test specimens depicted the MAFM process to be very effective in finishing hybrid Al/SiC/B_4C MMCs surfaces.

© 2025 Journal of Materials and Engineering

1. INTRODUCTION

The significance of surface finish quality and accuracy has grown as a result of rapid developments in engineering fields such as aircraft, automobile, electronics, medical (prosthetic knee joint implantation), optics and aerospace. Due to the rapid evolution of materials, the material characteristics including wear-resistance, toughness and hardness have gained popularity in the business. However, using conventional techniques to finish advanced materials is a difficult process and challenging to perform with tough materials. As a result, non-traditional finishing methods like abrasive flow machining, magnetorheological honing process, magnetic abrasive finishing and electrochemical magnetic abrasive finishing etc. have been developed recently. Non-traditional machining techniques have demonstrated their effectiveness for industrial use over the past few decades, particularly when new, exotic, and customized materials are manufactured. Magnetic abrasive flow machining (MAFM) is one of the cutting-edge machining approaches that meet the demands of the modern world. The basic operating principle of MAFM is demonstrated in Figure 1.

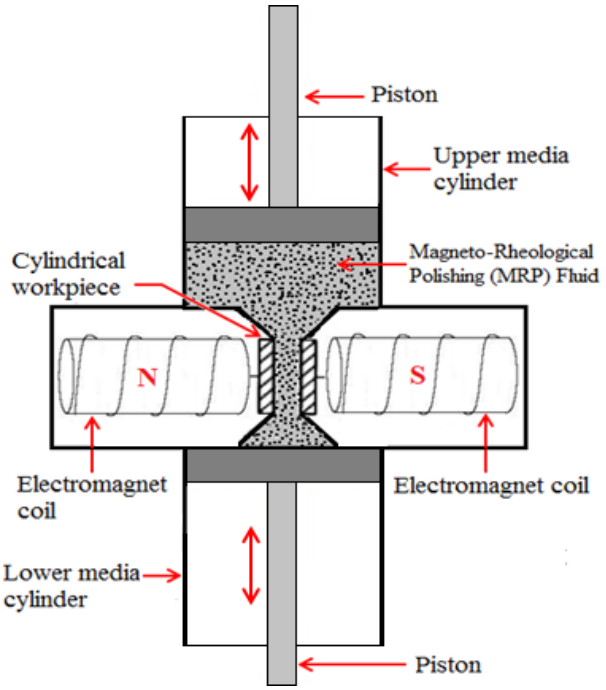


Fig. 1. Schematic diagram of MAFM principal.

The development of these techniques has significantly benefited the industries. Magneto-rheological polishing (MRP) fluid, sometimes referred to as abrasive media, is applied to the workpiece surface in MAFM. The MRP fluid, which contains the abrasive particles, abrades the roughness of the specimen surface under the influence of a strong magnetic flux density causing the material removal in the form of microchips. Over the years, MAFM has demonstrated its capability to finish components with exceptional quality, and it is appropriate for processing surfaces which are difficult to process by hand and have complex external and internal geometries. The past studies shed light on analyzing the machining process using various sets of parametric combinations to emphasize the significance of state-of-the-art machining in the current environment, as stated in the next section.

2. STATE OF THE ART REVIEW

The current study investigates the viability of using the MAFM process for improving the texture of inner cylindrical surface of hybrid Al/SiC/B_4C-MMCs using Fe-SiC bonded abrasives. The study indicates that no work has been done using the MAFM method to enhance the surface finish of hybrid Al/SiC/B_4C-MMCs. An adequate work has been carried out using various finishing processes and other abrasives like Al_2O_3, B_4C to finish several materials viz. aluminium, copper, brass, mild steel, stainless steel, HSS, Al/SiC-MMCs etc. An optimal set of input parameters are taken to reduce the surface roughness of Al/SiC/B_4C-MMCs. The six input parameters viz. magnetic flux density (M_f), workpiece material (W_p), number of cycles (N) concentration of abrasives (C), mesh number (M) and extrusion pressure (E_p) with three different levels are selected for the present experimental wok. For the process to be as effective as possible, process parameters must be optimized. Taguchi's L_{27} Orthogonal array has been employed to tackle this issue in the current study. The machined surfaces were compared with SEM before and after machining.

Authors/ Year	**Material**	**Experimental Design/Technique / Model/Method**	**Abrasives/ Media**	**Process Parameters**	**Responses Parameters**	**Findings**
Williams et.al (1992)	AISI 4140	Data dependent systems (DDS) methodology and scanning electron microscopy (SEM)	**Abrasive** Silicon carbide (SiC) **Media** Medium-high viscosity	Extrusion pressure, number of cycles, media viscosity	Metal removal rate (MRR), surface finish	The extrusion pressure and media viscosity were the most significant factors affecting MRR and surface finish [1].
Williams et al. (1998)	Stereolitho -graphy (SL)	A full factorial experiment design and SEM technique	SL 5170 photopolymer resin and 5180 photopolymer resin	Media pressure, grit size, resin type, build orientation and style	Flatness, MRR and surface roughness	Media pressure had a significant effect on MRR and the major enhancement in surface roughness was achieved through the initial AFM cycle [2].
Jain et al. (1999)	Mild steel	Response surface analysis	**Abrasive** Silicon carbide (SiC)	Number of cycles, mesh size, reduction ratio, percentage abrasive concentration and extrusion pressure	Material removal (MR) and change in surface roughness	The MR and change in surface roughness were increased with extrusion pressure, reduction ratio, number of cycles and percentage abrasive concentration [3].
Jain et al. (2000)	Aluminium	i) A generalized back-propagation neural network ii) Augmented lagrange multiplier iii) Genetic algorithm	**Abrasive** Silicon carbide (SiC)	Mesh size, number of cycles, abrasive concentration, and average piston velocity	MRR and surface roughness	The results found by GA were in favor with the optimized results obtained by neural network, which validated the neural network approach [4].
Jain et al. (2001)	Brass and Aluminum	–	**Abrasive** Silicon carbide (SiC) **Media** Bingham Plastic	Temperature of medium on the medium viscosity and mesh size and abrasive concentration	MR and surface roughness	A significant influence of media viscosity was obtained on MR and surface roughness as MR was increased and surface roughness was decreased by increasing the media viscosity [5].
Sehijpal et.al (2002)	Aluminum, Mild steel, Brass	Mixed factorial experimental design technique and SEM	**Abrasive** Aluminium oxide (Al_2O_3)	Extrusion pressure, average grain size, abrasive concentration, reduction ratio, media viscosity and volume flow rate	MR and surface roughness	The wear behavior of specific materials was analyzed by MAAFM process and a strong magnetization effect was observed on MR. SEM was also applied for analyzing the wear pattern of different material surfaces [6].
Gorana et.al (2004)	Mild steel	SEM and statistical 2^3 full factorial experimental technique	**Abrasive** Silicon carbide (SiC) **Media** Dow Corning 3179 dilatant compound (Silly putty)	Extrusion pressure, abrasive concentratio n and grain size	MR, reduction in surface roughness (Ra value), active grain density and cutting forces (radial and axial)	Abrasive concentration, extrusion pressure and grain size had a major influence on active grain density and cutting forces, due to which Ra value was reduced [7].

Singh et.al (2004)	Alloy steel (ferromagnetic)	Taguchi design of experiments using L_9 orthogonal array (OA)	Silicon carbide (SiC), ferromagnetic iron (Fe) and lubricant (SAE-30)	Abrasive size (mesh number), working gap, magnet rotational speed and DC voltage applied to the electromagnet	Change in surface roughness (ΔRa) and forces (cutting force and normal magnetic force)	The working gap and voltage were significant factors influencing the surface quality trailed by grain size and rotational speed [8].
Jayswal et al. (2005)	SUS 304 stainless steel	Galerkin's finite element method	**Abrasive** Aluminium oxide (Al_2O_3)	Abrasive particle size, power input, volume fraction, work piece size, finishing time, flux density, work piece material properties, rotating pole RPM, work piece initial surface roughness, magnetic abrasive particle size and properties	Volume of material removed and final surface roughness	A theoretical model was proposed for simulating MR and surface roughness in MAF process. On comparing the simulation results with experimental results, the simulated values were higher while the trend was same [9].
Gorana et al. (2006)	Mild steel and Aluminum	SEM technique	**Abrasive** Silicon carbide (SiC) **Media** (Abrasive & silly putty); (plain silly putty without abrasive)	Work piece material, abrasive grain, extrusion pressure, mesh number, abrasive concentration, media velocity w.r.t. workpiece and average initial surface roughness value	Active grain density, grain indentation depth, axial and radial force	A significant influence of radial force, axial force, grain depth of indentation and active grain density was observed on material deformation scale [10].
Gorana et al. (2006)	Mild steel	Analytical model	**Abrasive** Silicon carbide (SiC) **Media** Silly putty	Abrasive mesh size, extrusion pressure, initial workpiece roughness and abrasive concentration	Surface roughness (Ra) value	It was reported that the active grain density was improved with an increase in the percentage of media abrasive concentration and extrusion pressure during AFM process, due to which the percent reduction of Ra value was increased [11].

Wani et al. (2007)	Brass	Finite element model developed	**Abrasive** Magnetic abrasive particles (MAPs) made up of ferromagnetic particles (Fe) and abrasive grains (SiC, Al_2O_3 or diamond)	Number of cycle, magnetic flux density, media flow rate, diameter of abrasive and magnetic particle	MR, machining pressure and surface roughness	A good agreement was obtained among the simulation results and experimental results. A significant effect of magnetic field was found on MR and surface roughness [12].
Das et.al (2008)	Stainless-steel workpiece	Finite difference method	**Media** Magnetorheological polishing fluid (MRPF), a homogeneous mixture of abrasive particles and carbonyl iron particles in a base medium of paraffin liquid and grease	Number of cycles and magnetic flux density	Surface finish	The MRAFF was fabricated for finishing the nano parts and flow of media from the fixture was evaluated by a finite difference method. As a result a model was developed for predicting the values of MR and surface roughness [13].
Kar et al. (2009)	Aluminum, En8	–	**Abrasive** Silicon carbide (SiC) **Media** Vicso-elastic carriers (Natural rubber, styrene butadiene rubber, butyl rubber, silicone rubber, ethylene propylenediene monomer rubber, SiC abrasive and naphthenic oil	Number of cycles, abrasive concentration and workpiece	Percentage improvement in surface roughness (Ra)	A significant impact of creeping time, temperature, frequency and shear rate was found upon the rheological properties. Their relations trends were also governed by percentage ingredients of media. The surface roughness was increased by increasing the abrasive loading [14].
Fang et.al (2009)	AISI 1045, 1080 and A36 steels.	Computational fluid dynamics approach	**Abrasive** Boron carbide (B_4C) **Media** Three silicone rubbers with different mooney viscosity (15.4, 22.4, 23.0 at 20^0C temperature)	Media viscosity and number of cycles	Surface roughness (Ra) and MR	From AFM tests, it was reported that the MR and Ra were decreased with an increase in number of cycles. An additional improvement in Ra was observed with high viscosity media than low viscosity media during initial number of cycles [15].

Siddiqui et al. (2010)	Brass	Multi variable curve-fitting technique	**Abrasive** Silicon carbide (SiC) **Media** Waxpol polishing past, AP-3 grease and base oil	Media flow speed, number of cycles, abrasive concentration and mesh size	MR and Ra	The workpiece surface with single vent for outflow of media had a higher MR and a great improvement in Ra when compared with the workpiece having multiple vents [16].
Sadiq et al. (2010)	Mild steel (AISI 1020) Stainless steel (SS316L)	–	**Abrasive** Green SiC **Media** MR fluid made up of natural castor oil suspended with carbonyl iron particles treated through surfactant	Magnetic flux density, process duration, reciprocation frequency and rotation speed	Roughness and percentage change in roughness	A significant improvement in finishing proficiency of magnetorheological abrasive honing process was noticed by introducing the magnetic field around the non-magnetic workpieces that resulted in maximum 41.7% and 43.5% improvement in finishing [17].
Das et al. (2011)	Stainless steel	SEM, atomic force micrographs and central composite rotatable design (CCRD) of RSM	**Media** Magnetorheological polishing fluid (MRP), a homogeneous mixture of SiC abrasive particles and electrolytic Fe powder in a base medium of paraffin oil and AP3 grease	Extrusion pressure, finishing cycles, mesh size and magnet rotational speed	Change in out-of-roundness (ΔOOR) Rate of ΔOOR	It was revealed that roundness error of axisymmetric parts was reduced by using the R-MRAFF process, which improved the wear resistance and reliability (OOR = 2.04μm). A significant influence of magnet rotational speed was found i.e. OOR was improved by increasing the magnet rotational speed, while the improvement was reduced after a certain limit [18].
Brar et al. (2012)	Brass	Taguchi experiments design (L_8 OA)	**Abrasive** Aluminium oxide (Al_2O_3) **Media** Abrasive laden media	Extrusion pressure, media flow rate, helical drill bit status and number of cycles	MR and percentage improvement in surface roughness (ΔRa)	The improved fabricated helical abrasive flow machining (HLX-AFM) was developed that enhanced MR and ΔRa by using the helical twist drill bit that was fixed coaxially. After experimental work, it was reported that all process variables except extrusion pressure had a major effect upon the response variables [19].

Mulik et al. (2012)	AISI 52100 steel	Taguchi experiments design (L_{16} OA), developed mathematical models and SEM micrograph	**Abrasive** Silicon carbide (SiC) and Iron particles (Fe)	Electromagnet rotational speed, voltage supplied to electromagne, finishing gap, SiC abrasive weight percentage and pulse on time	Normal force and finishing torque	During ultrasonic assisted magnetic abrasive finishing (UAMAF) process, it was reported that the major factors affecting the supply voltage to electromagnet and finishing gap were finishing forces and torque. The investigational findings were matched with the developed models for normal force and finishing torque [20].
Harlal et al. (2012)	Al/SiC_p MMCs	Artificial neural networks (ANN)	**Abrasive** Silicon carbide (SiC) **Media** Blending of abrasives in polymer carrier with processing oil	Extrusion pressure, abrasive mesh size, media viscosity grade, abrasive percentage concentration and number of finishing cycles	Arithmetic mean value of surface roughness (Ra) and maximum peak–valley surface roughness height (Rt), and improvement in Rt and Ra	The results obtained from the trained neural model for finishing Al/SiCp-MMC were compared with the multivariable regression analysis results and validated prediction accuracy was obtained [21].
Judal et al. (2013)	Aluminium	–	**Abrasive** Steel grit and Al_2O_3 abrasives (magnetic abrasive particles)	Rotational speed, magnetic flux density, abrasive particles size and vibration frequency	MR and change in surface finish value (ΔRa)	A significant improvement in MR and surface roughness was obtained by investigating various process parameters using a novel vibration-assisted cylindrical-magnetic abrasive finishing (VAC-MAF) methodology [22].
Patil et al. (2014)	Copper	2^4 Fractional factorial design	**Abrasive** Silicon carbide (SiC) **Media** Blending of abrasive particles, modelling clay and varnish oil	Media flow speed, number of cycles, mesh size and abrasive concentration	Surface roughness	The effect of various process variables was studied and a mathematical relationship was observed among the surface roughness and process parameters. An improvement in machining capabilities was obtained with the newly developed technology using the optimized parameters [23].

Sangwan et al. (2015)	Ti-6Al-4V titanium alloy	Integrated artificial neural network, genetic algorithm (GA) and Taguchi's L_{27} OA methodology	–	Depth of cut (d), speed (v) and feed (f)	Surface roughness (Ra)	It was observed that the surface roughness was decreased by increasing the cutting speed and depth of cut. The main parameter influencing the minimization of surface roughness was feed [24].
Kathiresan et al. (2015)	Stainless steel- 304	Artificial neural network, regression models and Taguchi's L_{27} OA methodology	**Abrasive** Silicon carbide (SiC) **Media** Magnetorheological polishing (MRP) fluid was prepared by homogeneously mixing of carbonized iron particles, SiC particles and silicone oil	Hydraulic pressure, electromagnet current and number of cycles	surface roughness	On comparing the experimental and regression results of ANN, a close association was observed among the actual performance results and the predicted surface roughness value on validation [25].
Vaishya et al. (2015)	Gun metal	Taguchi L_9 OA	**Abrasive** Aluminium oxide (Al_2O_3) **Media** Abrasive particles, hydrocarbon gel, silicon based polymer and Non-Newtonian liquid polymer	Mesh Size, square CFG rod cross-section area, number of cycles and extrusion pressure	Surface finish (Ra)	It was reported using Taguchi's method that pressure had a significant percentage contribution of 37.60% using the hybrid AFM setup and number of cycles had 31.16% contribution for surface finish. It was also concluded that the surface finish was increased with an increase in number of cycles from 3 to 7 [26].
Seifu et al. (2016)	Mild steel	Computational fluid dynamic (CFD) analysis using ANSYS 15.0 software	**Abrasive** Silicon carbide (SiC) **Media** Polyborosiloxane with grease (carrier) impregnated with SiC	Volume fraction, abrasive size, pressure inlet, pressure outlet and media velocity	MRR, depth of indentation, axial stress and radial stress	The AFM modeling was presented that included the MRR and force modeling. CFD analysis was carried out and the simulation results of radial stress, axial stress, MRR and depth of indentation were found. From the result it was revealed that the axial force was greater than radial force for material removal [27].

Ali et al. (2016)	Aluminium	Taguchi L_9 OA, ANSYS 14 software and FLUENT software	**Abrasive** Carban nano tube (CNT) particles & alumina (Al_2O_3) **Media** Blending of alumina abrasive and polyborosilox ane with CNT particles	Extrusion pressure, amount of CNT particles and number of cycles	MR	From simulation results; it was observed that the temperature of media was enhanced by increasing the number of cycles, which varied the media viscosity. As a result the MR was initially increased till a certain limit and then it was decreased. However, by increasing the amount of CNT, the MR was increased [28].
Ahmad et al. (2017)	Stainless steel (202)	Taguchi L_9 OA and Minitab 15 software	**Abrasive** Iron powder (magnetic particles) and alumina powder **Media** Sintered magnetic abrasive (SMA) a mixture of alumina and cast iron powder with polyvinyl acetate (PVA)	Electromagn et voltage, machining gap, rotational speed, abrasive size and time	Change in roughness (ΔRa)	The experiments were performed using Taguchi's method and it was observed that the surface finish can be improved by the appropriate size of magnetic particles [29].
Verma et al. (2017)	Stainless steel (SS304)	RSM using central composite design and SEM technique	A variable magnetic flux density tool	Rotational speed, magnetic flux density, abrasive mesh number and weight percentage	Change in surface roughness percentage (%ΔRa)	The tool performance was evaluated by conducting the experiments using CCD technique and magnetic flux density was analyzed to be one of the most effective parameters during finishing of SS304 pipe [30].
Kathiresan et al. (2017)	AISI stainless steel 316L	RSM and SEM technique	**Media** Magnetorheo logical abrasive fluid {20% Fe particles, 20% SiC abrasive particles with 60% paraffin oil (base liquid) and a small amount of oleic acid as surfactant}	Hydraulic pressure, number of cycles and voltage	MRR and Surface roughness (SR)	An optimization firefly algorithm was used and it was observed that the electromagnet voltage was the major factor for producing the maximum MRR and a minimum SR. While a moderate contribution was made by hydraulic pressure and number of cycles [31].

Sambharia et al. (2017)	High speed steel (HSS)	Central composite rotatable design of RSM, SEM and XRD techniques	**Media** Highly viscous polymer abrasive gel (PAG)	Extrusion pressure, finishing time and viscosity of media	MR and improvement in surface roughness (ΔRa)	It was concluded that viscosity of media and finishing time had a major effect on finishing performance. As ΔRa was decreased, finishing time was increased while it was increased by increasing viscosity of media and extrusion pressure. On the other hand MR was increased with an increase in viscosity of media and extrusion pressure while it was decreased with an increase in finishing time. During the finishing of trim die surface, the highest value of MR and ΔRa was found 13.28 mg and 0.63 μm respectively [32].
Nagdeve et al. (2018)	Brass	–	**Abrasive** Corbonyl iron particles (CIPs), boron carbide (B_4C) **Media** Blending of abrasives with paraffin oil (carrier) and AP3 grease (surfactant)	MR fluid 1: CIPs (6 μm), B_4C (4 μm) MR fluid 2: CIPs (6 μm), B_4C (6 μm) MR fluid 3: CIPs (6 μm), B_4C (9 μm)	Percentage change in surface (%ΔRa) roughness and saturation magnetization (M) and yield stress	A higher yield stress was attained with the MR fluid having same size of particles (CIPs and B_4C) when compared with another combinations [33].
Petare et al. (2018)	Alloy steel 20MnCr5	Full factorial design of experiments and SEM technique	**Abrasive** Silicon carbide (SiC) **Media** Blending of abrasives with molding clay (silly putty) and silicone oil (blending oil)	Finishing time, extrusion pressure, media viscosity, hardness, abrasive particles (type, size and concentration), chemical composition and geometry of the straight bevel gears (SBG) material, fixture and clamping method	Deviations in pitch, SBG run out and surface finish	A precise coefficient was used for studying the wear mechanism and characteristics of the best finished SBGs and observed that micro-geometry, surface finish, quality of the bevel gears and wear characteristics were significantly improved by using the AFF process [34].

Singh et al. (2019)	Aluminum-6060	Taguchi L9 (OA), developed Buckingham-π dimensional model and SEM technique	**Abrasive** Unbonded type-magnetic abrasive particles, ferrous particles (Fe) and silicon carbide (SiC)	Rotational speed, abrasive weight, working gap and voltage	Rise in temperature and change in surface roughness (ΔRa)	The rise in surface temperature in mild steel was predicted using a semi empirical dimensional model. A maximum value for rise in temperature was attained as 9°C and for Al-6060 surface it was low [35].
Baraiya et al. (2020)	Aluminium alloy grade 6061	Taguchi L_{27} orthogonal array design, Minitab-17 statistical software,	**Abrasive** Silicon carbide (SiC) **Media** Silicone polymer-based abrasive media: a blend of abrasive particles with silicon-based polymer and hydrocarbon gel	Abrasive mesh size, Number of cycles and abrasive concentration in media, Other constant parameters are: extrusion force, abrasive Material, polymer to gel ratio, temperature, media flow volume per pass and stroke length	Percent improvement in surface roughness and change in surface roughness (ΔRa)	The results declared that the abrasives concentration, number of passes and abrasive mesh size had a major effect on ΔRa and highest percentage improvement of 35.71 %, 27.16 % and 37.89 % had been observed on the inner, side and outer surface respectively [36].
Yunus et al. (2020)	Al/SiC_p-MMCs	L_{27} OA and genetic programming (GP) approach	Abrasives in liquid silicon used as media for polishing the work-pieces.	Extrusion pressure, mesh number, abrasives concentration, number of cycles, workpiece material and oil in Media	MRR and surface roughness (ΔRa)	The finishing characteristics of Al/SiC_p-MMC were investigated using genetic programming and the results were simulated. By comparing the results with different modeling techniques, a higher degree of 99.97% accuracy was obtained [37].
Guo et al. (2020)	1.) Rapidly solidified aluminium (RSA)-905 2.) 6061-T6 aluminum or stavax	SEM and Vibration assisted magnetic abrasive polishing (VAMAP) method	**Abrasive** Iron powder and alumina powder	Finishing of curved rectangular micro features for ferrous as well as non-ferrous materials	Polishing forces, profile accuracy and lifetime test of abrasives, surface roughness, surface morphology and profile and magnetic field distribution analysis	The results revealed that the method employed for ferrous as well as non-ferrous materials having micro features was appropriate and an improvement in surface quality was observed with well-maintained micro features form [38].

Anjaneyulu et. al (2021)	Mild Steel (MS) plate	Grey relational analysis (GRA), Genetic algorithm (GA), and Jaya Algorithm (JA) techniques were used. Design of experiments with the help of L_9 orthogonal array. SEM analysis was conducted on MAF finished workpieces.	**Abrasives/ Media** Flexible Magnetic abrasive brush	Voltage, Speed of electromagnet and weight ratio of abrasives (%)	% of improvement of surface finish (% ΔRa)	Genetic algorithm (GA), grey relational analysis (GRA) and jaya algorithm (JA) were compared for analyzing the optimum solution by finishing the mild steel (MS) plate through MAF process. The regression equation attained through L_9 orthogonal array was used for optimizing the input variables like weight ratio of abrasives (%), speed of electromagnet and voltage to find their influence on the percentage of improvement of surface finish (% ΔR_a). Jaya algorithm was found to be the best optimization strategy and to offer the best overall solution when compared with other approaches [39].
Babbar et. al (2022)	Brass plate	Hybrid approach was used in which the Taguchi Technique (L_{16} orthogonal array) is employed in conjunction with multi-objective grey relational analysis technique.	**Magnetic Abrasives** Iron powder and Boron carbide powder	Spindle speed, the quantity of magnetic abrasives, mesh number and machining time.	Surface roughness (SR), Material removal rate (MRR)	A minimum surface roughness (0.066 µm) was reported at a machining time (60 min.), quantity of magnetic abrasives (5 mg), spindle speed (200 rpm), mesh number (#270), during finishing the brass plate with MAF process. A modest difference was determined among the experimental (0.9462) and expected findings (0.9009) for grey relational grade value [40].
Celik et. al (2022)	Ti6Al4V alloy	Taguchi L_{18} orthogonal array experimental design was used. Surface texture of specimens by SEM technique and EDX analysis	**Abrasives** Silicon carbide (SiC) and Iron particles (Fe). **Media** SAE 30 lubricant was used to keep the SiC and Fe particles together.	Machining time, abrasive particle size, the number of revolutions and magnetic field.	Surface roughness improvement rate (SRIR) and white layer thickness (WLTRR) (µm) of Magnetic abrasive finishing (MAF) / ultrasonic assisted magnetic abrasive finishing (UAMAF) experiments	During SEM analysis of the machined samples, variations in the thickness of the white layer were noted. The study revealed that using the MAF and UAMAF approaches, the white layer thickness could be reduced by 84% and 89%, respectively. Ultrasonic support was also found to have an average beneficial impact of 13.45% [41].

3. MATERIALS AND METHODS

The design and development of the experimental MAFM setup was executed in the laboratory. The MAFM experimental set-up specification is depicted in Table 1.

Table 1. Specifications of MAFM set-up.

S. No.	Specifications	Description	Units
1.	Maximum Extrusion Pressure	10	MPa
2.	Material of Hydraulic Cylinder	EN8	------
3.	Material of Piston	Grey Cast Iron	------
4.	Diameter of Hydraulic Cylinder	95	mm
5.	Diameter of Piston	90	mm
6.	Media Flow Volume per Pass	300	cm^3
7.	Stroke Length	250	mm
8.	Pressure Gauges	2 Nos.	(each 3000 psi)
9.	Pump	Hydraulic Gear Pump	------
10.	Motor	Flange type Motor	(2 H.P. and 1440 rpm)
11.	Fixture Material	Aluminium	------
12.	Temperature	32° C	(Room Temperature)
13.	Working Gap	1–2	mm
14.	Core size	Core length = 175	mm
		Radius of core = 25	mm
		Diameter of core rod = 35	mm
15.	Electromagnet coils	Coil weight = 3.820	kg
		Number of turns = 2500 per coil	------
		Coil material = 23 gauge copper wire	------
16.	Core material	Mild steel (M.S)	------
17.	Magnetic flux density (M_f)	0–2	Tesla
18.	DC power supply	0–240	Volt

The MAFM experimental setup, CAD model, schematic diagram and its flow chart is presented in Figure 2(a), Figure 2(b), Figure 2(c) and Figure 3 respectively. The workpiece was held by an aluminium fixture with slots, as seen in Figure 4(a). This was chosen because it was simple to machine and the slots could be precisely cut to fit the contour of the workpiece. The device slightly reduced the passage cross section to provide smooth medium passage with minimal vibration. The fixture and workpiece were removed after the specified number of cycles counted through a digital counter meter, and a new workpiece was inserted into the slots. The finished workpiece was washed through the acetone $(CH_3)_2CO$. The materials used for the workpiece are metal matrix composites (MMCs) having aluminium-6063 as the base material with SiC (9, 8, and 7%) and B_4C (1, 2, and 3%). Table 2 displays the proportional ratios of the constituents. To perform the experiments, three different test specimens were fabricated as casted rods of different compositions {Test Specimen-1: Al-6063/9 wt. % SiC/1 wt. % B_4C-MMC, Test Specimen-2: Al-6063/8 wt. % SiC/2 wt. % B_4C-MMC and Test Specimen-3: Al-6063/7 wt. % SiC/3 wt. % B_4C-MMC}.

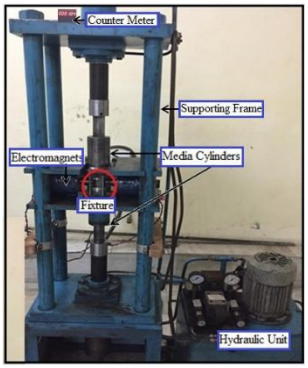


Fig. 2 (a). MAFM experimental set-up.

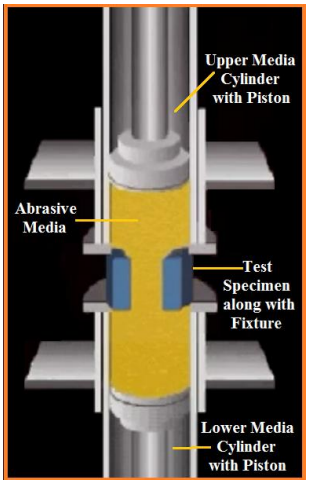


Fig. 2 (b). CAD Model.

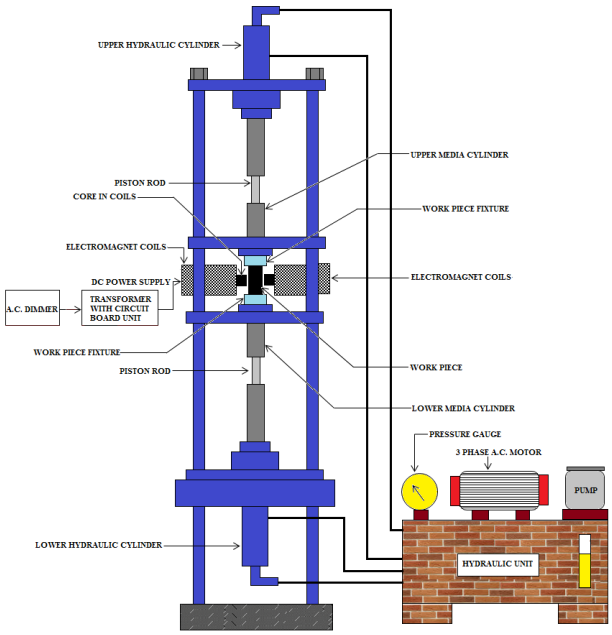


Fig. 2 (c). MAFM experimental set-up model.

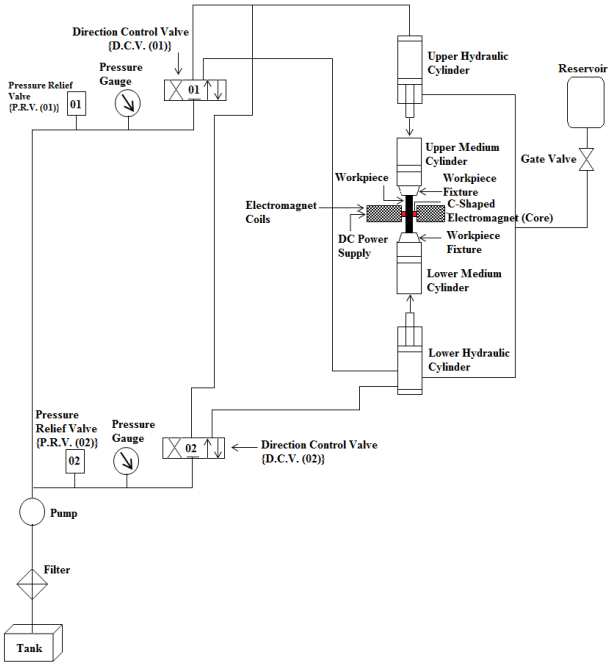


Fig. 3. Flow chart of MAFM Set-up

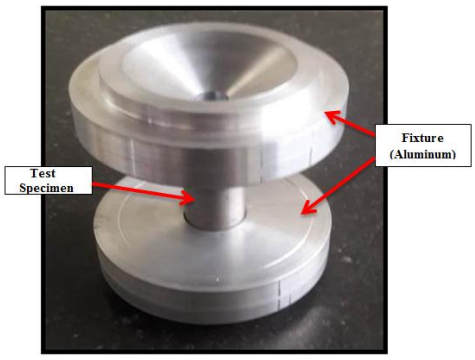


Fig. 4 (a). Aluminium fixture.

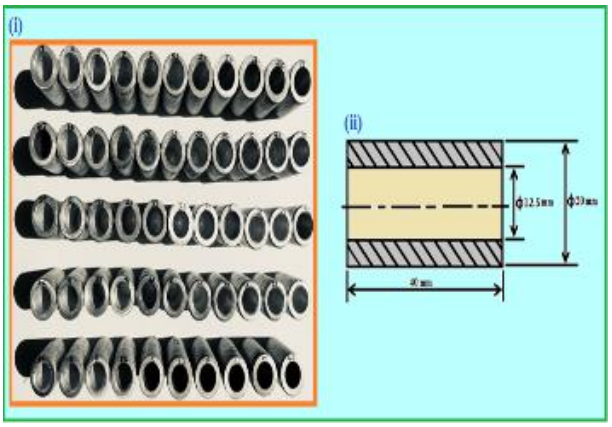


Fig. 4 (b). (i) Test specimens, (ii) Geometry of test specimen.

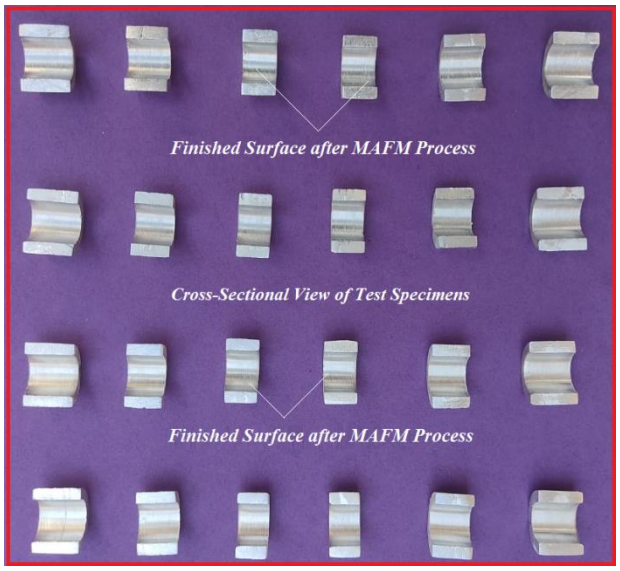


Fig. 4 (c). Finished test specimens (cross-sectional view) after MAFM process.

Table 2. Proportional ratios of constituents in workpiece materials.

Element	Specimen-1	Specimen-2	Specimen-3
Al-6063	Balance	Balance	Balance
Fe	0.28	0.16	0.18
Mg	0.76	0.53	0.72
Cu	0.03	0.02	0.04
Si	9.15	8.02	6.82
Zn	0.0010	0.0012	0.0012
Mn	0.0064	0.0050	0.0068
Pb	0.0025	0.0026	0.0027
B	1.01	1.96	2.86
Cr	0.0016	0.0021	0.0021
Ti	0.0096	0.0090	0.0091

The inner cavity of the test specimens to the required size {internal diameter (12.5 mm), external diameter (20 mm) and length (40 mm)} was prepared [19, 26, 28, 42–47] by drilling operation followed by boring operation before finishing with MAFM process as depicted in Figure 4(b). Figure 4(c) depicts the cross-sectional view of the finished test specimens. In order to prepare the media, hydraulic oil, liquid silicon rubber (carrier), abrasive particles (SiC) and iron (Fe) particles were uniformly mixed. A dummy workpiece was used as a conduit for the media to be thoroughly mixed. Table 3 depicts the abrasive media used during experimental work. Al/SiC/B_4C MMCs were used as the workpieces in the pilot experimentation that employed the one-variable-at-a-time (OVAT) technique. Magnetic flux density (M_f), workpiece material (W_p), mesh number (M), concentration of abrasives (C), extrusion pressure (E_p) and number of cycles (N) were used as input parameters whereas MRR and ΔRa were used as output parameters. Table 4 illustrates the parameters used and their levels based on pilot experiments and a thorough literature review.

Table 3. Composition of MRP Fluid (Media).

S. No.	Constituents	Value of the constituents	% Volume concentration in media
1.	Hydraulic oil	68 number	10%
2.	Liquid silicon rubber (Carrier)	White colour (RTV-2615)	35%, 30%, 25%
3.	Silicon carbide (SiC) abrasive particle	150 mesh size 220 mesh size 400 mesh size	45%, 50%, 55%
4.	Iron (Fe) particle	300 mesh size	10%

Table 4. Input parameters and their levels.

Symbols	Input parameters	Level			Units
		I	II	III	
A	Magnetic flux density (M_f)	0.15	0.3	0.45	Tesla
B	Workpiece material (W_p)	1	2	3	Type
C	Mesh number (M)	150	220	400	Nos.
D	Concentration of abrasives (C)	45	50	55	Wt. %
E	Extrusion pressure (E_p)	3	5	7	Mpa
F	Number of cycles (N)	100	150	200	Nos.

4. DESIGN OF EXPERIMENTS

The design of experiment is an essential phase in the majority of experimental based research studies. Establishing the relationship among input and response parameters is the goal of experimentation. Taguchi's L_{27} Orthogonal array was employed for the experimentation and each experiment was run three times. The experiments were conducted utilizing various input process parameter values provided by the Taguchi L_{27} array. Table 5 and 6 provides the computed MRR and ΔR_a values.

4.1 Material removal rate measurement (MRR; µg/sec)

For measuring the weight of each sample, BL-220H, an electronic balance with 10^{-3} g accuracy was employed. The material removal value for every experiment (before and after finishing with MAFM) is evaluated by following equation:

$$\text{MRR} = \frac{(\text{Initial weight} - \text{Final weight})}{\text{Time}} \quad (1)$$

4.2 Change in surface roughness measurement (ΔR_a; µm)

The roughness of the workpiece surface was calculated by E35-B, a digital handysurf machine for every initial and final sample. The change in surface roughness value for every experiment (before and after finishing with MAFM) is evaluated by following equation:

$$\Delta R_a = R_{a\,(initial)} - R_{a\,(final)} \quad (2)$$

$R_{a\,(initial)}$ = Surface roughness (before finishing with MAFM)
$R_{a\,(final)}$ = Surface roughness (after finishing with MAFM)

5. RESULTS AND DISCUSSIONS

5.1 Main effect and Interaction plots

In the MAFM setup, a magnetic effect is applied around the test specimen, causing the polishing fluid to get stiff. An increase in magnetic effect from 0.15 to 0.45 Tesla causes more metal removal by the abrasives from the surface asperities. This is because of the

development of iron particle chains, which surround the surface microscopic irregularities [12–13, 17, 22, 30, 40–41]. As a result, the mean value of MRR and ΔR_a is enhanced as depicted in Figure 5 and 6 respectively.

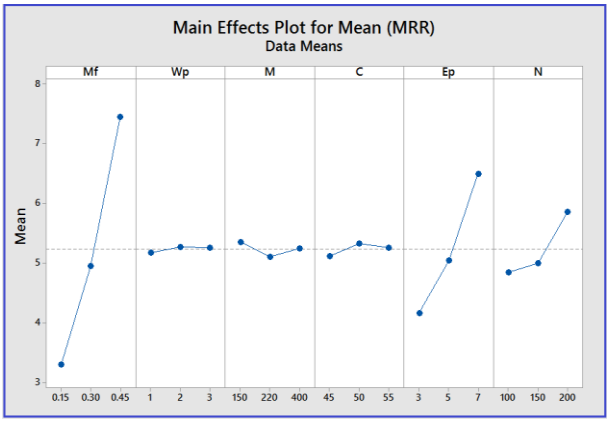


Fig. 5. Main effects plot for means (MRR).

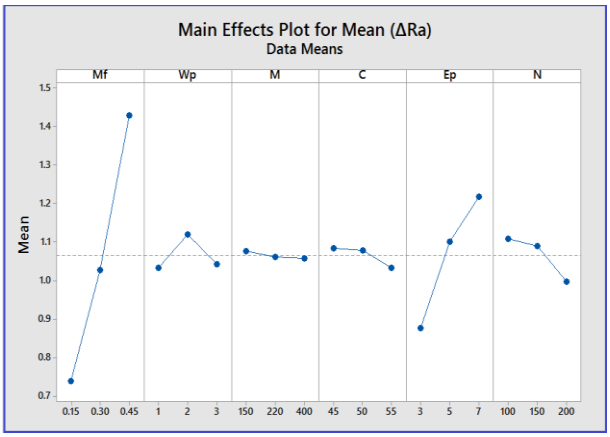


Fig. 6. Main effects plot for means (ΔR_a).

Moreover, the findings of this investigation showed that increasing the extrusion pressure value (3 to 7 Mpa) increases both MRR and ΔR_a as demonstrated in Figure 5 and 6 respectively. This occurs due to more abrasion with permitted abrasive particles having increased extrusion pressure since these particles have a higher impact on the surface [1, 3, 6–7, 10–11, 18–19, 21, 25–26, 28, 31–32, 34, 37].

Moreover, the value of MRR increases with an increase in the number of cycles from 100 to 200 as depicted in Figure 5. This is due to the fact that more peaks are sheared off and deeply penetrated during the abrasion process when the large number of abrasive particles is present. As a result, during the finishing process, more material is removed from the workpiece surface. However, because there are more peaks and valleys in the initial stages of machining therefore, ΔR_a initially improves. As the number of cycles is further increased, smaller peaks are machined, becoming somewhat flatter than previously [1, 3–4, 12–19, 21, 23, 25–26, 28, 31, 36–37]. As a result, ΔR_a decreases as depicted in Figure 6. According to ANOVA Table 9 and 10, Figure 5 and 6 it has been observed that mesh number (M), concentration of abrasives (C) and workpiece material (W_p) had little impact on MRR and ΔR_a.

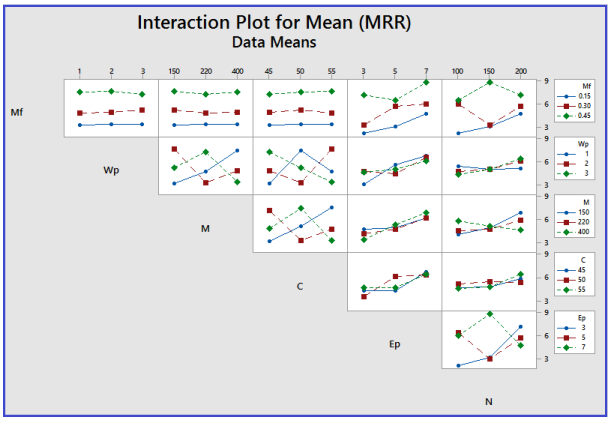


Fig. 7. Interactions plot for means (MRR).

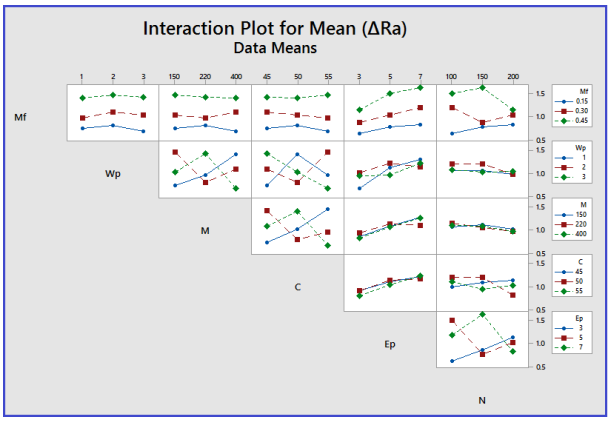


Fig. 8. Interactions plot for means (ΔR_a).

Figure 7 and 8 depict the interaction plots for MRR and ΔR_a respectively. The optimal combination of process variables for MRR is M_{f3} W_{p2} M_1 C_2 E_{p3} N_3 and for ΔR_a is M_{f3} W_{p2} M_1 C_1 E_{p3} N_1 as observed from Figure 5 and 6.

5.2 Analysis of signal to noise (S/N) ratio

Table 5 and 6 show the experimental data of MRR, ΔR_a and S/N ratio for magnetic abrasive flow machining of Al/SiC/B_4C workpieces with Fe-SiC bonded abrasives. The 'larger the better' criteria is employed to compute the 'S/N ratio' for both MRR and ΔR_a. The main effect plot for the 'S/N ratios' of MRR is depicted in Figure 9.

It can be clearly seen from Figure 9 that magnetic flux density (M_f) is the most important factor, followed by extrusion pressure (E_p) and number of cycles (N) influencing the MRR. The best combination of levels for control parameters from the analysis that provides a maximum MRR, was found at magnetic flux density (M_f) = 0.45 Tesla, workpiece material (W_p) = 3, mesh number (M) = 150, concentration of abrasives (C) = 50, extrusion pressure (E_p) = 7 Mpa and number of cycles (N) = 200.

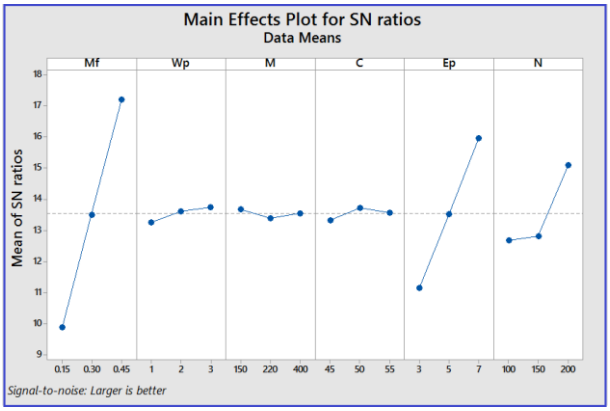


Fig. 9. Main effects plot for S/N ratios (MRR).

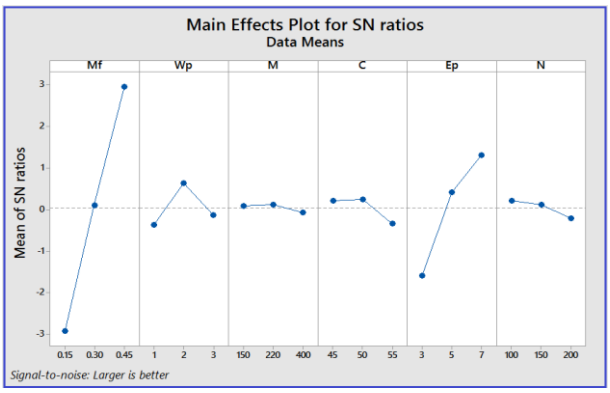


Fig. 10. Main effects plot for S/N ratios (ΔR_a).

The main effect plot for the 'S/N ratios' of ΔR_a is depicted in Figure 10. It can be clearly seen from Figure 10 that magnetic flux density (M_f) is the most important factor, followed by the extrusion pressure (E_p) and number of cycles (N) influencing the ΔR_a. The best combination of levels for control parameters from the analysis that provides a maximum ΔR_a, was found at magnetic flux density (M_f) = 0.45 Tesla, workpiece material (W_p) = 2, mesh number (M) = 220, concentration of abrasives (C) = 50, extrusion pressure (E_p) = 7 Mpa and number of cycles (N) = 100.

Table 5. L_{27} orthogonal arry (Experimental Results for MRR; µg/s).

Run No.	Factors						MRR1 (10^{-6} g/s)	MRR2 (10^{-6} g/s)	MRR3 (10^{-6} g/s)	Mean (MRR)	S/N Ratio
	M_f	W_p	M	C	E_p	N					
1	0.15	1	150	45	3	100	1.92	1.98	1.78	1.89	5.53
2	0.15	1	150	45	5	150	2.52	2.90	3.09	2.84	9.07
3	0.15	1	150	45	7	200	4.71	5.13	5.21	5.02	14.01
4	0.15	2	220	50	3	100	1.81	2.02	2.69	2.17	6.73
5	0.15	2	220	50	5	150	2.65	3.98	3.11	3.25	10.24
6	0.15	2	220	50	7	200	3.99	4.97	4.57	4.51	13.08
7	0.15	3	400	55	3	100	1.99	2.43	2.81	2.41	7.64
8	0.15	3	400	55	5	150	2.67	2.89	3.31	2.96	9.43
9	0.15	3	400	55	7	200	4.44	4.89	4.73	4.69	13.42
10	0.3	1	220	55	3	150	2.81	2.49	2.96	2.75	8.79
11	0.3	1	220	55	5	200	5.19	5.63	6.01	5.61	14.98
12	0.3	1	220	55	7	100	5.81	6.33	5.92	6.02	15.59
13	0.3	2	400	45	3	150	2.79	3.01	3.72	3.17	10.02
14	0.3	2	400	45	5	200	5.59	4.50	3.99	4.69	13.42
15	0.3	2	400	45	7	100	6.43	7.41	6.58	6.80	16.65
16	0.3	3	150	50	3	150	3.89	3.12	3.96	3.66	11.27
17	0.3	3	150	50	5	200	6.89	6.61	6.87	6.79	16.64
18	0.3	3	150	50	7	100	5.39	5.01	4.99	5.13	14.20
19	0.45	1	400	50	3	200	4.86	5.13	4.11	4.70	13.44
20	0.45	1	400	50	5	100	8.98	8.01	8.14	8.38	18.46
21	0.45	1	400	50	7	150	9.79	8.99	9.52	9.43	19.49
22	0.45	2	150	55	3	200	8.91	9.12	8.87	8.97	19.06
23	0.45	2	150	55	5	100	5.77	5.12	5.23	5.37	14.60
24	0.45	2	150	55	7	150	8.78	8.31	8.66	8.58	18.67
25	0.45	3	220	45	3	200	7.95	8.04	7.45	7.81	17.85
26	0.45	3	220	45	5	100	5.12	5.89	5.56	5.52	14.84
27	0.45	3	220	45	7	150	7.99	8.89	8.25	8.38	18.46

Table 6. L_{27} orthogonal arry (Experimental Results for ΔR_a; μm)

Run No.	Factors						ΔR_a1 (μm)	ΔR_a2 (μm)	ΔR_a3 (μm)	Mean (ΔR_a)	S/N Ratio
	M_f	W_p	M	C	E_p	N					
1	0.15	1	150	45	3	100	0.49	0.39	0.45	0.44	–7.13
2	0.15	1	150	45	5	150	0.81	0.74	0.78	0.78	–2.16
3	0.15	1	150	45	7	200	0.73	1.32	0.91	0.99	–0.09
4	0.15	2	220	50	3	100	0.66	1.31	0.59	0.85	–1.41
5	0.15	2	220	50	5	150	0.85	0.99	1.05	0.96	–0.35
6	0.15	2	220	50	7	200	0.44	0.74	0.63	0.60	–4.44
7	0.15	3	400	55	3	100	0.54	0.61	0.59	0.58	–4.73
8	0.15	3	400	55	5	150	0.69	0.51	0.48	0.56	–5.04
9	0.15	3	400	55	7	200	0.67	1.05	0.96	0.89	–1.01
10	0.3	1	220	55	3	150	0.58	0.75	0.66	0.66	–3.61
11	0.3	1	220	55	5	200	0.85	1.05	1.19	1.03	0.26
12	0.3	1	220	55	7	100	1.10	1.18	1.29	1.19	1.51
13	0.3	2	400	45	3	150	0.81	0.95	1.21	0.99	–0.09
14	0.3	2	400	45	5	200	1.06	1.21	1.12	1.13	1.06
15	0.3	2	400	45	7	100	1.09	1.16	1.24	1.16	1.29
16	0.3	3	150	50	3	150	0.84	0.98	1.03	0.95	–0.45
17	0.3	3	150	50	5	200	0.83	0.89	1.03	0.92	–0.72
18	0.3	3	150	50	7	100	1.31	1.22	1.13	1.22	1.73
19	0.45	1	400	50	3	200	0.85	0.99	0.94	0.93	–0.63
20	0.45	1	400	50	5	100	1.59	1.42	1.63	1.55	3.81
21	0.45	1	400	50	7	150	1.78	1.69	1.71	1.73	4.76
22	0.45	2	150	55	3	200	1.03	1.31	1.19	1.18	1.44
23	0.45	2	150	55	5	100	1.69	1.61	1.41	1.57	3.92
24	0.45	2	150	55	7	150	1.71	1.54	1.66	1.64	4.30
25	0.45	3	220	45	3	200	1.38	1.23	1.33	1.31	2.35
26	0.45	3	220	45	5	100	1.49	1.32	1.42	1.41	2.98
27	0.45	3	220	45	7	150	1.53	1.40	1.69	1.54	3.75

5.3 Analysis of variance

ANOVA is a method of designing experiments that divides total variance into its underlying variation causes. The factors are analyzed as well as the effect of independent variables on the dependent variables is evaluated using the ANOVA technique. ANOVA and the statistical framework for creating the experiments were first introduced by British biologist Sir Ronald A. Fisher. It is a mathematical technique for analyzing experimental data and making decisions about the elements being investigated. The Taguchi method has been employed on MINITAB software to perform the analysis of variance. Table 7 and 8 list the MRR and ΔR_a average values (means) respectively at every level for each of the six variables.

ANOVA Table 9 depicts that for MRR, magnetic flux density (M_f) is the highly significant factor, followed by the extrusion pressure (E_p), the number of cycles (N) while a little effect of concentration of abrasives (C), workpiece material (W_p) and the mesh number (M) has been obtained on MRR. The contribution of every factor is: magnetic flux density (M_f = 58.57%), extrusion pressure (E_p = 18.52%), the number of cycles (N = 3.47%), concentration of abrasives (C = 0.06%), workpiece material (W_p = 0.02%) and the mesh number (M = 0.01%) as presented in Table 9. ANOVA Table 10 depicts that for ΔR_a, magnetic flux density (M_f) is the most important factor, followed by the extrusion pressure (E_p), the number of cycles (N) while a minute effect of concentration of abrasives (C), mesh number (M) and the workpiece material (W_p) has been attained on ΔR_a. The contribution of every factor is: magnetic flux density (M_f = 66.35%), extrusion pressure (E_p = 16.22%), the number of cycles (N = 1.69%), concentration of abrasives (C = 0.35%), workpiece material (W_p =0.04%) and the mesh number (M = 0.01%) as presented in Table 10.

Table 7. Response Table for Means (MRR).

Level	M_f	W_p	M	C	E_p	N
1	3.304	5.182	5.361	5.124	4.170	4.854
2	4.958	5.279	5.113	5.336	5.046	5.002
3	7.460	5.261	5.248	5.262	6.507	5.866
Delta	4.156	0.097	0.248	0.211	2.337	1.011
Rank	1	6	4	5	2	3

Table 8. Response Table for Means (ΔR_a).

Level	M_f	W_p	M	C	E_p	N
1	0.7389	1.0333	1.0767	1.0833	0.8767	1.1078
2	1.0278	1.1200	1.0611	1.0789	1.1011	1.0900
3	1.4289	1.0422	1.0578	1.0333	1.2178	0.9978
Delta	0.6900	0.0867	0.0189	0.0500	0.3411	0.1100
Rank	1	4	6	5	2	3

Table 9. Analysis of variance (ANOVA) for MRR.

Source	D.F.	Seq. SS	Contribution	Adj. SS	Adj. MS	F-Value	P-Value	Remarks
Regression	6	107.007	80.66%	107.007	17.8345	13.90	0.000	
M_f	1	77.709	58.57%	77.709	77.7089	60.56	0.000	Highly significant
W_p	1	0.028	0.02%	0.028	0.0280	0.02	0.884	
M	1	0.014	0.01%	0.014	0.0139	0.01	0.918	
C	1	0.085	0.06%	0.085	0.0854	0.07	0.799	
E_p	1	24.570	18.52%	24.570	24.5700	19.15	0.000	significant
N	1	4.601	3.47%	4.601	4.6006	3.59	0.073	significant
Error	20	25.665	19.34%	25.665	1.2832			
Total	26	132.672	100.00%					

Table 10. Analysis of variance (ANOVA) for (ΔR_a).

Source	D.F.	Seq. SS	Contribution	Adj. SS	Adj. MS	F-Value	P-Value	Remarks
Regression	6	2.73335	84.65%	2.73335	0.45556	18.38	0.000	
M_f	1	2.14245	66.35%	2.14245	2.14245	86.44	0.000	Highly significant
W_p	1	0.00036	0.01%	0.00036	0.00036	0.01	0.906	
M	1	0.00124	0.04%	0.00124	0.00124	0.05	0.826	
C	1	0.01125	0.35%	0.01125	0.01125	0.45	0.508	
E_p	1	0.52361	16.22%	0.52361	0.52361	21.12	0.000	significant
N	1	0.05445	1.69%	0.05445	0.05445	2.20	0.154	significant
Error	20	0.49573	15.35%	0.49573	0.02479			
Total	26	3.22907	100.00%					

Table 11. Model Summary for MRR.

Model	S	R-Sq.	R-Sq. (adj.)	PRESS	R-sq. (pred.)
Summary	1.13280	80.66%	74.85%	49.2794	62.86%

Table 12. Model Summary for ΔR_a.

Model	S	R-Sq.	R-Sq. (adj.)	PRESS	R-sq. (pred.)
Summary	0.157437	84.65%	80.04%	0.890377	72.43%

By raising the magnetization effect from 0.15 to 0.45 Tesla, more metal is eliminated by the media from the surface asperities. This causes an increased value of MRR and ΔR_a, improving the surface finish quality. These results affirmed the conclusions made by Shan et al. [47]. In addition, according to the findings of the current study, increasing the value of the extrusion pressure causes an increase in both MRR and ΔR_a. This occurs as more abrasion is caused with enabled abrasive particles that have higher extrusion pressure because these particles impact the surface with greater impact. These results support the findings that Jain et al. [48–50] have reported. Also, with an increase in the number of cycles, the MRR and ΔR_a were increased initially due to the presence of more peaks and valleys. However, the value of MRR and ΔR_a was reduced with further increase in the number of cycles as there were lesser peaks to be machined. These results validate the research results presented by Shan and Wang [47–48].

5.4 Regression analysis

For quantitative variables, the regression technique is proved to be quite beneficial. The prediction of response to repeated levels of the variables can be done on the basis of the model. The input and response parameters are analyzed and a relationship among them is formulated using Minitab software. In the present study, the input parameters are the Magnetic flux density (M_f), Workpiece material (W_p), Mesh number (M), Concentration of abrasives (C), Extrusion pressure (E_p) and Number of cycles (N). The material removal rate (MRR) and change in surface roughness (ΔR_a) are the response parameters. Equations (3) and (4) provide the linear regression model developed in this work. Table 11 and 12 shows the model summary statistics for all responses.

Regression Equation for MRR

Mean (MRR) = – 4.06 + 13.85 × Magnetic flux density (M_f) + 0.039 × Workpiece material (W_p) – 0.00022 × Mesh number (M) + 0.0138 × Concentration of abrasives (C) + 0.584 × Extrusion pressure (E_p) + 0.01011 × Number of cycles (N) (3)

Regression Equation for ΔR_a

Mean = 0.371 + 2.300 × Magnetic flux density (M_f) + 0.0044 × Workpiece material (W_p) – 0.000064 × Mesh number (M) – 0.00500 × Concentration of abrasives (C) + 0.0853 × Extrusion pressure (E_p) – 0.001100 × Number of cycles (N) (4)

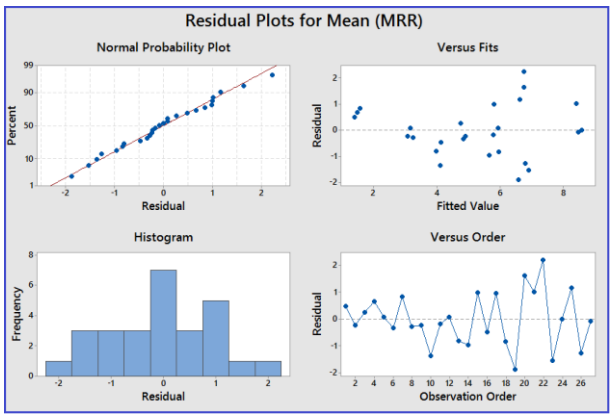


Fig. 11. Residual plots for mean (MRR).

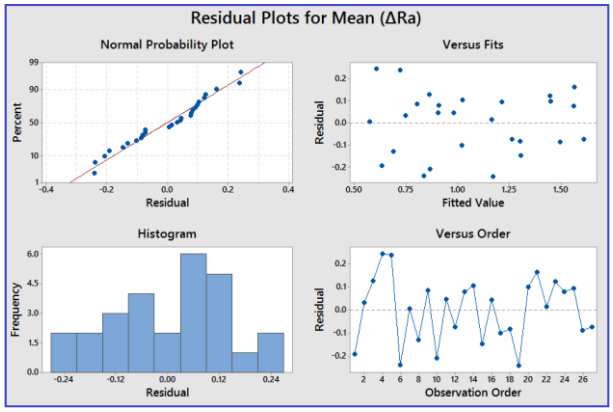


Fig. 12. Residual plots for mean (ΔR_a)

In Figures 11 and 12, the residual plot for the procedure's means is displayed. These plots depict that the normal probability plot indicates the normal distribution of data resembling a straight line, suggesting that the factors influence the response. When comparing residuals to fitted values, it can be seen that the residuals have little scatter and are represented as a band with a little incline in the middle, centered about zero. This leads us to the conclusion that the error variance is nearly constant. The residues are found to be dispersed and lack any discernible pattern, proving that the errors are independent and the data is not skewed, which supports the applicability of the model.

5.5 Confirmation test and optimum levels

The purpose of the confirmatory experiment is to confirm that the experimental findings are accurate. When employing partial factorial designs and orthogonal arrays (OA), confirmation is necessary because there are aliases and confusion with the OA columns. The MINITAB software offers an ideal value for the process variable while taking into account the findings of the experimental data. The optimal level combination for the specified control parameters in MRR is the magnetic flux density (M_f) = 0.45 Tesla, workpiece material (W_p) = 3, mesh number (M) = 150, concentration of abrasives (C) = 50, extrusion pressure (E_p) = 7 Mpa and number of cycles (N) = 200. The ideal set of operations for MRR is denoted by the acronym M_{f3} W_{p2} M_1 C_2 E_{p3} N_3. Moreover, the optimal level combination for the specified control parameters in ΔR_a is the magnetic flux density (M_f) = 0.45 Tesla, workpiece material (W_p) = 2, mesh number (M) = 220, concentration of abrasives (C) = 50, extrusion pressure (E_p) = 7 Mpa and number of cycles (N) = 100. Also, the ideal set of operations for ΔR_a is denoted by the acronym M_{f3} W_{p2} M_1 C_1 E_{p3} N_1. A final test was conducted under ideal circumstances to verify the accuracy of the model. The test conditions and MRR which are predicted by the model and determined experimentally are depicted in Table 13.

Table 13. Confirmation test result for MRR.

Process Parameters	Optimum conditions						Value of response (MRR)		
	M_f	W_p	M	C	E_p	N	Observed values	Predicted values	Percent error (%)
Value	0.45	3	150	50	7	200	8.72	8.51	2.41

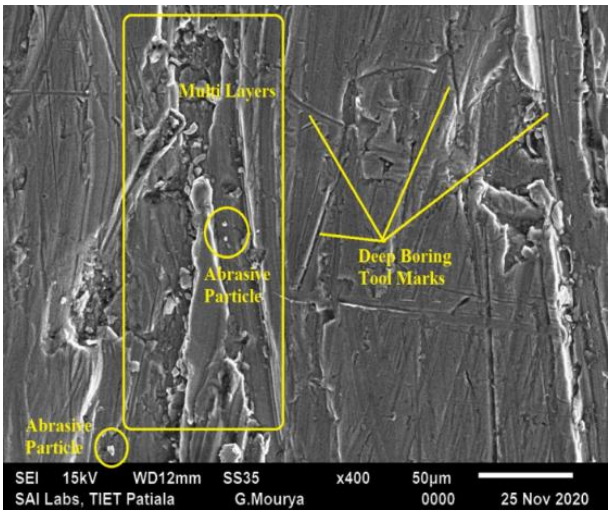
Table 14. Confirmation test result for ΔR_a.

Process Parameters	Optimum conditions						Value of response (MRR)		
	M_f	W_p	M	C	E_p	N	Observed values	Predicted values	Percent error (%)
Value	0.45	2	200	50	7	100	1.83	1.75	4.37

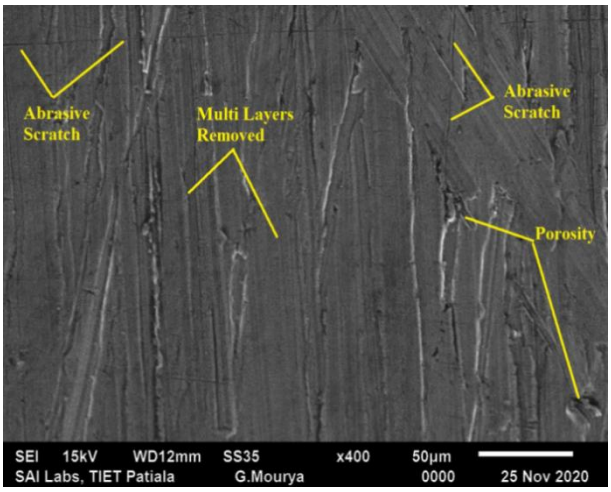
It comes out that MRR can be predicted by the model with an error of 2.41%. The test conditions and ΔR_a which are predicted by the model and determined experimentally are depicted in Table 13. Additionally, it comes out that ΔR_a can be predicted by the model with an error of 4.37%.

6. MICROSTRUCTURE ANALYSIS

Surface morphology of the test specimens before and after finishing with MAFM was analyzed by scanning electron microscopy (SEM) at magnification ×400 and the photographs are depicted in Figures 13, 14, and 15. From the SEM image (Figure 13(a)), it can be clearly seen that the surface has deep boring tool marks and multi layers which have been removed after finishing as the surface is relatively smoother (Figure 13(b)). Additionally, it was noted that the surface of the specimen had some abrasive particles lodged in it. Moreover, Figure 14(c) displays the results of the surface test conducted before finishing, while Figure 14(d) depicts the outcome of the finished surface.

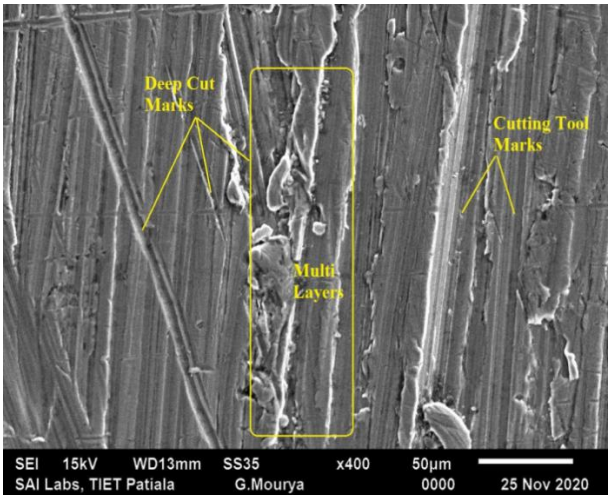


(a)

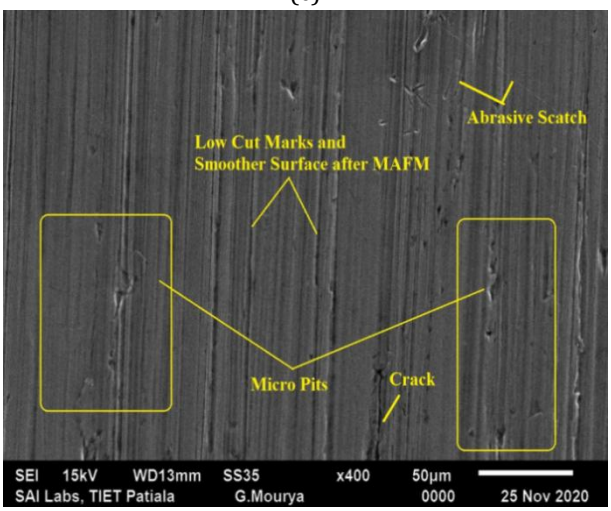


(b)

Fig. 13. SEM micrograph of (a) unfinished and (b) finished Al-6063 / SiC (9 wt. %) / B_4C (1 wt. %)-MMC (Test Specimen-1).

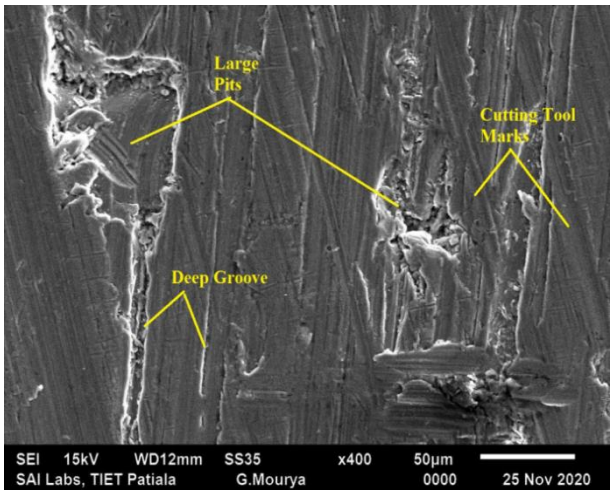


(c)

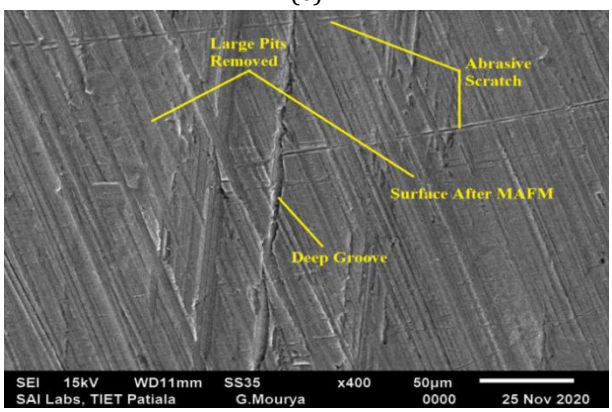


(d)

Fig. 14. SEM micrograph of (c) unfinished and (d) finished Al-6063 / SiC (8 wt. %) / B_4C (2 wt. %)-MMC (Test Specimen-2).



(e)



(f)

Fig. 15. SEM micrograph of (e) unfinished and (f) finished Al-6063 / SiC (7wt. %) / B_4C (3 wt. %)-MMC (Test Specimen-3).

The topographic curve in Figure 14(c) shows a rough surface with a big peak to valley height; in contrast, the topographic curve in Figure 14(d) shows a smooth surface with a significant peak to valley height reduction. Figure 15(e) depicts that large pits, cutting tool marks and deep grooves were present on the surface before finishing which have been removed after finishing with MAFM as the surface is relatively flatter (Figure 15(f)). These results demonstrate that the final surface was considerably smoother than it was initially, indicating that the MAFM process is particularly effective at reducing the surface roughness of test specimens.

7. CONCLUSION

From this study, the following observations can be drawn:

1. Magnetic flux density and extrusion pressure were found to be the most significant factors for MRR and ΔR_a based on the results of an ANOVA. Both MRR and ΔR_a were increased by increasing the magnetic flux density and extrusion pressure.
2. MRR and ΔR_a were enhanced initially by increasing the number of cycles. A further increase in the number of cycles reduced the value of ΔR_a as there were lesser peaks and valleys.
3. According to ANOVA it has been observed that mesh number (M), concentration of abrasives (C) and workpiece material (W_p) had a little impact on MRR and ΔR_a.
4. The best combination of levels for control parameters from the analysis that provides a maximum MRR, was found at magnetic flux density (M_f) = 0.45 Tesla, workpiece material (W_p) = 3, mesh number (M) = 150, concentration of abrasives (C) = 50, extrusion pressure (E_p) = 7 Mpa and number of cycles (N) = 200.
5. The best combination of levels for control parameters from the analysis that provides a maximum ΔR_a, was found at magnetic flux density (M_f) = 0.45 Tesla, workpiece material (W_p) = 2, mesh number (M) = 220, concentration of abrasives (C) = 50, extrusion pressure (E_p) = 7 Mpa and number of cycles (N) = 100.
6. The range of the MRR was found to be between 1.89 and 9.43×10^{-6} g/s. The confirmation experiment determined the optimal MRR to be 8.72×10^{-6} g/s, and predicted value to be 8.51×10^{-6} g/s. The difference among the predicted and experimental outcomes has a 2.41 percent error.
7. ΔR_a had a range of 0.44 to 1.73 m. The confirmation experiment revealed that the optimal ΔR_a was 1.83 as compared to the predicted value of 1.75 m. The difference in percentage between experimental and predicted outcomes is 4.37.
8. Microscopic captured images of final surfaces demonstrate how effective the MAFM technique is in finishing the hybrid Al/SiC/B_4C MMC surfaces.

Acknowledgement

The National Institute of Technology (NIT), Kurukshetra, Haryana, India, provided the necessary facilities for the current study endeavour, for which the authors are grateful. The authors are also grateful to Thapar University Patiala, Punjab, India, for allowing them to use the facilities in their lab (SEM and EDX). From any organisation or institution, no financial support has been given.

REFERENCES

[1] R. E. Williams and K. P. Rajurkar, "Stochastic modeling and analysis of abrasive flow machining," *Journal of Engineering for Industry*, vol. 114, no. 1, pp. 74–81, Feb. 1992, doi: 10.1115/1.2899761.

[2] R. E. Williams and V. L. Melton, "Abrasive flow finishing of stereolithography prototypes," *Rapid Prototyping Journal*, vol. 4, no. 2, pp. 56–67, Feb. 1998, doi: 10.1108/13552549810207279.

[3] R. K. Jain and V. K. Jain, "Simulation of surface generated in abrasive flow machining process," *Robotics and Computer Integrated Manufacturing*, vol. 15, no. 5, pp. 403–412, Oct. 1999, doi: 10.1016/S0736-845(99)00046-0.

[4] R. K. Jain and V. K. Jain, "Optimum selection of machining conditions in abrasive flow machining using neural network," *Journal of Materials Processing Technology*, vol. 108, no. 1, pp. 62–67, Dec. 2000, doi: 10.1016/S0924-0136(00)00621-X.

[5] V. K. Jain, C. Ranganatha and K. Muralidhar, "Evaluation of rheological properties of medium for AFM process," *Machining Science and Technology*, vol. 5, no. 2, pp. 151–170, Feb. 2007, doi: 10.1081/MST-100107841.

[6] S. Sehijpal, H. S. Shan and P. Kumar, "Wear behavior of materials in magnetically assisted abrasive flow machining," *Journal of Material Processing Technology*, vol. 128, no. 1–3, pp. 155–161, Oct. 2002, doi: 10.1016/S0924-0136(02)00442-9.

[7] V. K. Gorana, V. K. Jain and G. K. Lal, "Experimental investigation into cutting forces and active grain density during abrasive flow machining," *International Journal of Machine Tools and Manufacture*, vol. 44, no. 2–3, pp. 201–211, Feb. 2004, doi: 10.1016/j.ijmachtools.2003.10.004.

[8] D. K. Singh, V. K. Jain and V. Raghuram, "Parametric study of magnetic abrasive finishing process," *Journal of Materials Processing Technology*, vol. 149, no. 1–3, pp. 22–29, Feb. 2004, doi: 10.1016/j.jmatprotec.2003.10.030.

[9] S. C. Jayswal, V. K. Jain and P. M. Dixit, "Modeling and simulation of magnetic abrasive finishing process," *The International Journal of Advanced Manufacturing Technology*, vol. 26, pp. 477–490, Feb. 2005, doi: 10.1007/s00170-004-2180-x.

[10] V. K. Gorana, V. K. Jain and G. K. Lal, "Forces prediction during material deformation in abrasive flow machining," *Wear*, vol. 260, no. 1–2, pp. 128–139, Jan. 2006, doi: 10.1016/j.wear.2004.12.038.

[11] V. K. Gorana, V. K. Jain and G. K. Lal, "Prediction of surface roughness during abrasive flow machining," *The International Journal of Advanced Manufacturing Technology*, vol. 31, pp. 258–267, May. 2006, doi: 10.1007/s00170-005-0197-4.

[12] A. M. Wani, V. Yadava and A. Khatri, "Simulation for the prediction of surface roughness in magnetic abrasive flow finishing (MAFF)," *Journal of Materials Processing Technology*, vol. 190, no. 1–3, pp. 282–290, Jul. 2007, doi: 10.1016/j.jmatprotec.2007.02.036.

[13] M. Das, V. K. Jain and P. S. Ghoshdastidar, "Fluid flow analysis of magnetorheological abrasive flow finishing (MRAFF) process," *International Journal of Machine Tools and Manufacture*, vol. 48, no. 3–4, pp. 415–426, Mar. 2008, doi: 10.1016/j.ijmachtools.2007.09.004.

[14] K. K. Kar, N. L. Ravikumar, P. B. Tailor, J. Ramkumar and D. Sathiyamoorthy, "Performance evaluation and rheological characterization of newly developed butyl rubber based media for abrasive flow machining process," *Journal of Materials Processing Technology*, vol. 209, no. 4, pp. 2212–2221, Feb. 2009, doi: 10.1016/j.jmatprotec.2008.05.012.

[15] L. Fang, J. Zhao, K. Sun, D. Zheng and D. Ma, "Temperature as sensitive monitor for efficiency of work in abrasive flow machining," *Wear*, vol. 266, no. 7–8, pp. 678–687, Mar. 2009, doi: 10.1016/j.wear.2008.08.014.

[16] S. S. Siddiqui, and M. Hameedullah, "Abrasive flow machining performance measures on work-piece surfaces having different vent/passage considerations for media-outflow," 2010. semanticscholar.org/paper/Abrasive-flow-machining-performance-measures-on-for-Siddiqui Hameedullah/ed40fac698bd5d9caf19c1a551a2c956ee3c3e58

[17] A. Sadiq and M. S. Shunmugam, "A novel method to improve finish on non-magnetic surfaces in magneto-rheological abrasive honing process," *Tribology International*, vol. 43, no. 5–6, pp. 1122–1126, May–Jun. 2010, doi: 10.1016/j.triboint.2009.12.038.

[18] M. Das, V. K. Jain and P. Ghoshdastidar, "The out-of-roundness of the internal surfaces of stainless steel tubes finished by the rotational–magnetorheological abrasive flow finishing process," *Materials and Manufacturing Processes*, vol. 26, no. 8, pp. 1073–1084, Aug. 2011, doi: 10.1080/10426914.2010.537141.

[19] B. S. Brar, R. S. Walia, V. P. Singh and M. Sharma, "Helical abrasive flow machining (HLX-AFM) process," International Journal of Surface Engineering & Materials Technology, vol. 2, no. 2, pp. 48–52, Jul.–Dec. 2012. [Online]. Available: https://somme.in/admin/upload/pdf/03%20IJSEMT%20Vol2No2Jul-Dec2012-50-54.pdf

[20] R. S. Mulik and P. M. Pandey, "Experimental investigations and modeling of finishing force and torque in ultrasonic assisted magnetic abrasive finishing," *Journal of Manufacturing Science and Engineering*, vol. 134, no. 5, pp. 051008 (12 pages), Oct. 2012, doi: 10.1115/1.4007131.

[21] S. M. Harlal, and A. Manna, "Simulation of surface generated during abrasive flow finishing of Al/SiCp-MMC using neural networks," *The International Journal of Advanced Manufacturing Technology*, vol. 61, pp. 1263–1268, Apr. 2012, doi: 10.1007/s00170-012-4091-6.

[22] K. B. Judal, V. Yadava and D. Pathak, "Experimental investigation of vibration assisted cylindrical–magnetic abrasive finishing of aluminum workpiece," *Materials and Manufacturing Processes*, vol. 28, no. 11, pp. 1196–1202, Nov. 2013, doi: 10.1080/10426914.2013.811725.

[23] V. B. Patil, A. S. Bhanage and R. S. Patil, "Analysis and optimization of process parameters of abrasive flow machining process for super finishing of non-ferrous material nozzle," *Applied Mechanics and Materials*, vol. 612, pp. 97–104, Aug. 2014, doi: 10.4028/www.scientific.net/AMM.612.97.

[24] K. S. Sangwan, S. Saxena and G. K. Garg, "Optimization of machining parameters to minimize surface roughness using integrated ANN-GA approach," *Procedia CIRP*, vol. 29, pp. 305–310, Dec. 2015, doi: 10.1016/j.procir.2015.02.002.

[25] S. Kathiresan, K. Hariharan and B. Mohan, "Prediction of surface roughness in magneto rheological abrasive flow finishing process by artificial neural networks and regression analysis," *Applied Mechanics and Materials*, vol. 766–767, pp. 1076–1084, June. 2015, doi: 10.4028/www.scientific.net/AMM.766-67.1076.

[26] R. O. Vaishya, R. S. Walia and P. Kalra, "Parametric investigation of gun metal for surface roughness with hybrid abrasive flow machining process," *International Journal of Multidisciplinary and Current Research*, vol. 3, pp. 736–741, Jul.–Aug. 2015.

[27] Y. Seifu, K. S. Santhosh and S. S. Hiremath, "Modeling and simulation: machining of mild steel using indigenously developed abrasive flow machine," *Procedia Technology*, vol. 25, pp. 1312–1319, Dec. 2016, doi: 10.1016/j.protcy.2016.08.230.

[28] P. Ali, R. S. Walia, V. Rastogi and M. Tyagi, "Modelling of CNT particles based abrasive laden media used for abrasive flow machining," *Proceedings of 6th International & 27th All India Manufacturing Technology, Design and Research Conference*. ISBN: 978-93-86256-27-0: 178–183

[29] S. Ahmad, S. Gangwar, P. C. Yadav and D. K. Singh, "Optimization of process parameters affecting surface roughness in magnetic abrasive finishing process," *Materials and Manufacturing Processes*, vol. 32, pp. 1723–1729, Feb. 2017, doi: 10.1080/10426914.2017.1279307.

[30] G. C. Verma, P. Kala and P. M. Pandey, "Experimental investigations into internal magnetic abrasive finishing of pipes," *The International Journal of Advanced Manufacturing Technology*, vol. 88, no. 5–8, pp. 1657–1668, Feb. 2017, doi: 10.1007/s00170-016-8881-0.

[31] S. Kathiresan and B. Mohan, "Experimental analysis of magneto rheological abrasive flow finishing process on AISI stainless steel 316L," *Materials and Manufacturing Processes*, vol. 33, no. 4, pp. 422–432, Feb. 2017, doi: 10.1080/10426914.2017.1279317.

[32] J. K. Sambharia, H. S. Mali and V. Garg, "Experimental investigation on unidirectional abrasive flow machining of trim die work piece," *Materials and Manufacturing Processes*, vol. 33, no. 6, pp. 651–660, Feb. 2017, doi: 10.1080/10426914.2017.1364847.

[33] L. Nagdeve, A. Sidpara, V. K. Jain and J. Ramkumar, "On the effect of relative size of magnetic particles and abrasive particles in MR fluid-based finishing process," *Machining Science and Technology*, vol. 22, no. 3, pp. 493–506, Sep. 2017, doi: 10.1080/10910344.2017.1365899.

[34] A. C. Petare and N. K. jain, "On simultaneous improvement of wear characteristics, surface finish and microgeometry of straight bevel gears by abrasive flow finishing process," *Wear*, vol. 404–405, no. 15, pp. 38–49, Jun. 2018, doi: 10.1016/j.wear.2018.03.002.

[35] R. K. Singh, S. Gangwar and D. K. Singh, "Experimental investigation on temperature affected magnetic abrasive finishing of aluminum 6060," *Materials and Manufacturing Processes*, vol. 34, no. 11, pp. 1274–1285, Jun. 2019, doi: 10.1080/10426914.2019.1628263.

[36] R. Baraiya, A. Babbar, V. Jain and D. Gupta, "In-situ simultaneous surface finishing using abrasive flow machining via novel fixture," *Journal of Manufacturing Processes*, vol. 50, pp. 266–278, Feb. 2020, doi: 10.1016/j.jmapro.2019.12.051.

[37] M. Yunus and M. S. Alsoufi, "Genetic based experimental investigation on finishing characteristics of AlSiCp-MMC by abrasive flow machining," *International Journal of Engineering and Technology Innovation*, vol. 10, no. 4, pp. 293–305, Sep. 2020, doi: 10.46604/ijeti.2020.4951.

[38] J. Guo, W. Feng, H. J. H. Jong, H. Suzukic and R. Kanga, "Finishing of rectangular microfeatures by localized vibration-assisted magnetic abrasive polishing method," *Journal of Manufacturing Processes*, vol. 49, pp. 204–213, Jan. 2020, doi: 10.1016/j.jmapro.2019.11.026.

[39] K. Anjaneyulu and G. Venkatesh, "Optimization of process parameters of magnetic abrasive finishing using Jaya algorithm," *Materials Today: Proceedings*, vol. 41, no. 5, pp. 1035–1040, Jul. 2020, doi: 10.1016/j.matpr.2020.06.568.

[40] A. Babbar, A. Sharma and P. Singh, "Multi-objective optimization of magnetic abrasive finishing using grey relational analysis," *Materials Today: Proceedings*, vol. 50, no. 5, pp. 570–575, Mar. 2021, doi: 10.1016/j.matpr.2021.01.004.

[41] M. Celik, H. Gurun and U. Caydas, "Surface modification of wire-EDMed Ti6Al4V alloy by ultrasonic assisted magnetic abrasive finishing technique," *Surface Topography: Metrology and Properties*, vol. 10, no. 2, pp. 1–15, May 2022, doi: 10.1088/2051-672X/ac68fe.

[42] R. S. Walia, H. S. Shan and P. Kumar, "Abrasive flow machining with Additional centrifugal force Applied to the media," *Machining Science and Technology*, vol. 10, no. 3, pp. 341–354, Jul. 2006, doi: 10.1080/10910340600902157.

[43] R. S. Walia, H. S. Shan and P. Kumar, "Enhancing AFM process productivity through improved

fixturing," *The International Journal of Advanced Manufacturing Technology*, vol. 44, no. 7, pp. 700–709, Oct. 2009, doi: 10.1007/s00170-008-1893-7.

[44] R. S. Walia, "Development and Investigations in Centrifugal Force Assisted Abrasive Flow Machining Process," Ph.D. dissertation, Dept. Mechanical and Industrial Eng., IIT, Roorkee, Uttarakhand, 2006.

[45] B. S. Brar, R. S. Walia, V. P. Singh and M. Sharma, "Development of a robust abrasive flow machining process setup," *International Journal of Surface Engineering and Materials Technology*, vol. 1, no. 1, pp. 17–23, Jul.–Dec. 2011.

[46] B. S. Brar, R. S. Walia, V. P. Singh and M. Sharma, "A robust helical abrasive flow machining (HLX-AFM) process," *Journal of the Institution of Engineers (India): Series C.*, vol. 94, no. 1, pp. 21–29, Mar. 2013, doi: 10.1007/s40032-012-0054-9.

[47] H. S. Shan and S. Singh, "Development of magneto abrasive flow machining process," *International Journal of Machine Tools and Manufacture*, vol. 42, no. 8, pp. 953–959, June 2002, doi: 10.1016/S0890-6955(02)00021-4.

[48] A. C. Wang and S. H. Weng, "Developing the polymer abrasive gels in AFM process," *Journals of Materials Processing Technology*, vol. 192–193, no. 1, pp. 486–490, Oct. 2007, doi: 10.1016/j.jmatprotec.2007.04.082.

[49] R. K. Jain, V. K. Jain and P. M. Dixit, "Modeling of material removal and surface roughness in Abrasive flow machining process," *International Journal of Machine Tools & Manufacture*, vol. 39, no. 12, pp. 1903–1923, Dec. 1999, doi: 10.1016/S0890-6955(99)00038-3.

[50] V. K. Jain and S. G. Adsul, "Experimental investigations into abrasive flow machining (AFM)," *International Journal of Machine Tools & Manufacture*, vol. 40, no. 7, pp. 1003–1021, May 2000, doi:10.1016/S0890-6955(99)00114-5.